Supporting Information

Colloidally Assembled Zinc Ferrite Magnetic Beads: Superparamagnetic Labels with High Magnetic Moments for MR sensors

Jooneon Park,[a,d] Marc D. Porter,[a,b,d] and Michael C. Granger[a,c,d,§,]*

[a]Department of Chemical Engineering, The University of Utah
[b]Department of Chemistry, The University of Utah
[c]Department of Surgery, School of Medicine, The University of Utah
[d]Nano Institute of Utah, The University of Utah

Table of Contents

1. Experimental details

1.1. Assay substrate configuration and fabrication

The design and layout of the assay substrates, which consists of alternating nickel and gold addresses, are shown in **Figure S1D**. **Figure S1D** shows the entire substrate: twelve gold addresses are interspersed between thirteen nickel addresses. Both nickel and gold addresses are 200 × 200 μm in size. Each gold address is spaced (edge to edge) 500 μm from its neighboring nickel addresses. The nickel and gold addresses are used for reference magnetic signals and assay areas, respectively.[1-3]

The assay substrate was created using photolithographic and lift-off techniques. The detailed preparation of the assay substrate can be found elsewhere.[1-3] Briefly, the assay substrates were fabricated by evaporating nickel (10-nm thick) and gold (200-nm thick) addresses on Pyrex wafers (2-mm thick). Prior to the evaporation of nickel and gold, a 10-nm thick chromium layer was deposited as an adhesion layer. To prevent possible oxidation of nickel addresses, a 15-nm thick titanium layer was overlaid on the nickel addresses. In the next step, the entire wafer was coated with parylene, which was then removed from the gold addresses by plasma etching. The wafer was then diced into individual 0.3 × 2.0 cm rectangular sticks (the substrate).

1.2. MR sensor and station

The MR sensor was provided by NVE Corp., the details of which have been described elsewhere, along with those for the magnetics test station.[2-4] The sensor (**Figure S1C**) is designed as an integrated circuit of four resistors in a Wheatstone bridge configuration. The two interdigitated resistors function as a sense pad (200 × 200 μm in size). The other two resistors act as reference resistors, which have 30-μm offsets from the sense pad. The MR sensors are coated with a 250-nm protective layer of silicon nitride (Si_3N_4).

The MR station provides for relative motion between the assay substrate and MR sensor in the directions of *x*-, *y*- and *z*-axes as described in **Figure S2**. For readout, the sensor was placed between two electromagnetic coils (Nicollet Technologies Corp., Minneapolis, MN) in a Helmholtz configuration. Once an assay substrate was placed inverted above the sensor, the separation distance (*d*, *z*-axis) between the sensor and assay substrate was adjusted by a four-phase stepper motor (STMicroelectronics L298N). Because the MR signal magnitude is

dependent on *d*, it is critical to maintain a constant *d* throughout the substrate scanning. Also, the tilt angle of the assay substrate in the *z*-axis was manipulated by an Oriel controller, which has a resolution of (2.0 ± 0.1) × 10^{-3} degree per step, in order to prevent a change in *d* across the assay substrate while scanning. This process of changing the tilt angle was used to adjust the assay substrate until the plane of the substrate was parallel to the *x*-*y* plane of the MR sensor pad. Tilt in *y*-axis was manually aligned. To measure MR signals, the translation of the sensor across the assay substrate in the *x*-axis was controlled by a micromanipulator (Model 6000, Micromanipulator Co., Carson City, NV) with a second four-stage stepper motor.

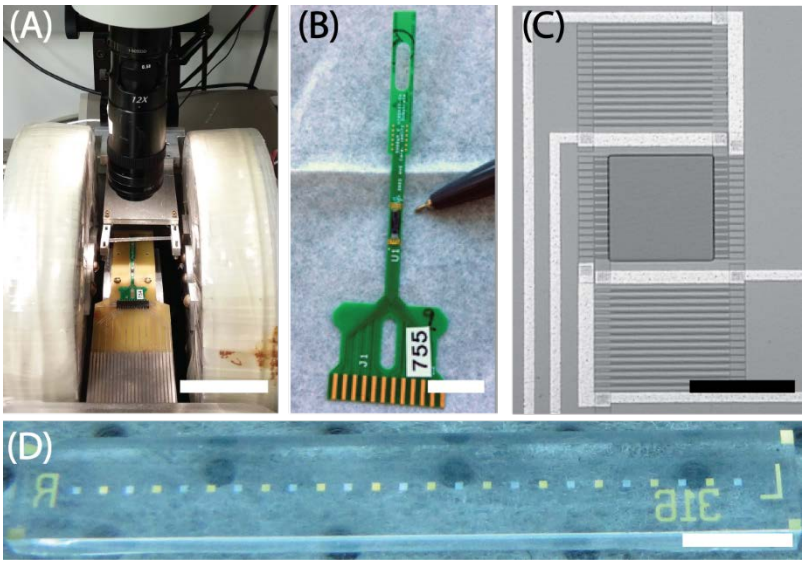

Figure S1. MR station, MR sensor, and assay substrate. (A) Image of actual MR station. Scale bar is 6 cm. (B) Image of MR sensor mounted on the green PCB board. The ink pen points to the sensor. Scale bar is 1 cm. (C) Image of MR sensor pad. The active sensing area is the square area in the middle. Scale bar is 200 μm. (D) Image of the assay substrate showing alternating nickel and gold addresses. Scale bar is 3 mm.

1.3. MR signal analysis method

To measure MR signals, an applied field of 100 Oe was chosen after careful characterization of the transfer curve and noise of the MR sensor. The *d* between the substrate and MR sensor was set at 10 ± 1.0 μm. The translational scanning speed of the assay substrate along the addresses was 31.1 ± 0.1 μm/sec.

In order to quantitatively measure MR responses, we incorporate magnetic reference addresses (*i.e.*, nickel addresses).[1-2] The MR signals from nickel addresses not only account for any change in *d*, but also provides for normalization of the MR signal from each gold address. As illustrated in **Figure S2B**, the

normalized response ($\boldsymbol{MR}_{norm,i}$) from the *i*th gold address with respect to the two Ni addresses in closest proximity can be written as follows,

$$\boldsymbol{MR}_{norm,i} = \frac{2\Delta E_{Au,i}}{\Delta E_{Ni,i-1}+\Delta E_{Ni,i+1}} \quad \textbf{(equation S1)}$$

where ΔE_{Au} and ΔE_{Ni} represent the responses (voltage changes) of gold and nickel addresses, respectively.

The MR response for each antigen concentration was determined by averaging the MR responses from twelve replicates gold addresses on one substrate. Similarly, the standard deviation for each MR data point was obtained from the twelve gold addresses on each substrate.

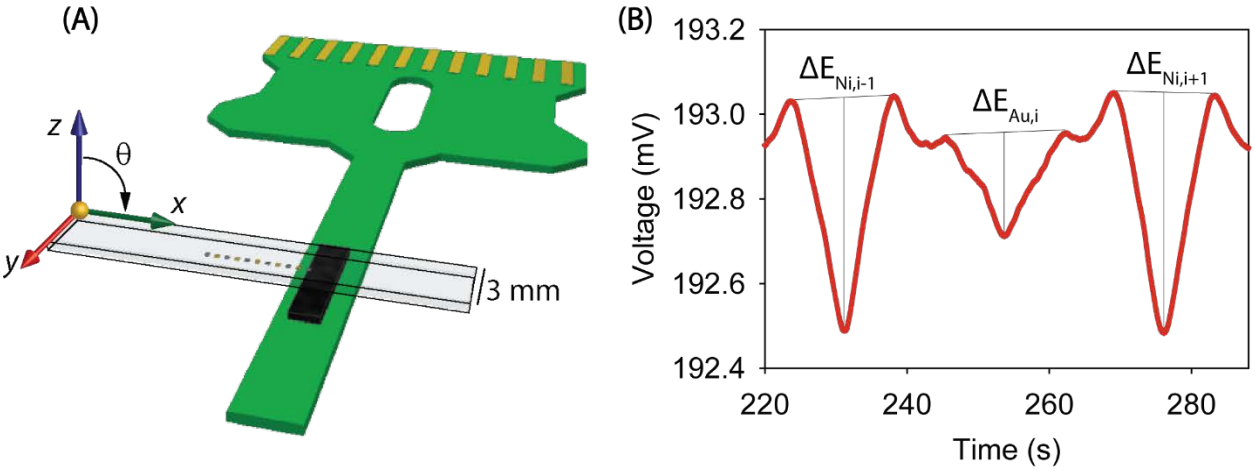

Figure S2. Schematic illustration of (A) substrate scanning above MR sensor, and (B) MR signal processing.

1.4. Sample characterizations and measurements

Scanning (SEM) and transmission electron microscopy (TEM): SEM images were collected using a Hitachi S-4800 (Japan), which was equipped with an energy dispersive X-ray spectroscopy module (EDS, INCA Inc.). Particle samples were prepared by dropcasting onto a 1×1 cm silicon chip for SEM imaging and EDS. TEM samples were prepared by dropcasting onto a 3-mm lacey carbon grid and images were obtained using JEM-2800 (JEOL, Japan). For the estimation of average particle size, ImageJ was used and at least 250 particles were measured for each sample.

Infrared (IR) spectroscopy: IR transmission spectra were obtained using a Nicolet Magna 850 Fourier transform IR spectrometer. The particle samples were dispersed in a KBr pellet at the concentration of ~1% (w/w). Spectra were collected using 512 scans at a resolution of 1 $cm.^{-1}$

Hydrodynamic size, zeta (ζ)-potential measurement, and nanoparticle tracking analysis: A Zetasizer Nano (Malvern Instruments, United Kingdom) with a disposable folded capillary cell was used to measure the zeta (ζ)-potential and hydrodynamic sizes of the suspended particles. At least three measurements per sample (n=3) were taken to calculate average values of hydrodynamic size and ζ-potential. A system of nanoparticle tracking analysis (NanoSight LM10, Malvern Instruments, United Kingdom) was used to measure the concentration of magnetic labels. At least three aliquots per magnetic label were measured to estimate the average concentration of magnetic labels.

Vibrating sample magnetometry (VSM): Magnetic hysteresis measurements were performed with a vibrating sample magnetometer (VSM EZ7, MicroSense, Lowell, MA) at room temperature.

Fluorescent microscopy: A fluorescent microscope (BX50WI, Olympus, Japan) equipped with a fluorescent cube (U-N41012) and a 12.8 megapixel CCD camera (DP72) was used to capture fluorescent images of FITC-avidin tagged ZFMB labels. A droplet of the FITC-avidin tagged ZFMB labels was sandwiched between a microscope glass slide and cover slip for imaging.

Inductively coupled plasma mass spectroscopy (ICP-MS): Inductively coupled plasma collision cell quadrupole mass spectrometer (Agilent 7500ce) was used to determine the composition of Zn and Fe in the ZFNPs. Dried ZFNPs were digested in 3 mL concentrated HCl and 1 mL concentrated HNO_3 (trace metal grade) and diluted with 5% HNO_3 to about 200 ppb Fe and 10 ppb Zn. A calibration solution containing 200 ppb Fe and 10.0 ppb Zn was prepared using single element standard solutions (Inorganic Ventures). Diluted sample and calibration solution were run together using a double-pass spray chamber, quartz injector, and platinum cones. Collision cell flushed with He (8 mL/min) was used in order to decrease the $^{40}Ar^{16}O$ interference at mass 56.

2. Estimation of magnetic moment per particle

To estimate magnetic moment per particle, $\boldsymbol{m}_{particle}$, two main assumptions were used: (1) surface capping molecules are negligible, and (2) the densities of the ZFNPs, Turbobead®, and Dynabead® are equal to magnetite, cobalt, and the value given by the vendor, respectively. The $\boldsymbol{m}_{particle}$ is calculated based on 1 g of the sample. The calculation for $\boldsymbol{m}_{particle}$ of the Dynabeads is given as an example. The diameter (D) and density (ρ) of the Dynabeads provided by the vendor are 1.05 μm and 1.8 g/cm^3, respectively. Assuming the particle is spherical, the volume per particle ($V_{particle}$) is given by:

$$V_{particle} = \frac{1}{6}\pi D^3 = 6.06\times10^{-12}\ cm^3 \qquad \textbf{(equation S2)}$$

Using the density, the mass per particle ($W_{particle}$) can also be estimated as:

$$W_{particle} = V_{particle}\times \rho = 1.09\times10^{-12}\ g/particle \qquad \textbf{(equation S3)}$$

The mass magnetization at 100 Oe ($\sigma_{s,100\ Oe}$, emu/g) for Dynabeads, determined by our VSM, is 6.21. Therefore, the $\boldsymbol{m}_{particle}$ of Dynabead at 100 Oe can be obtained by multiplying $W_{particle}$ and $\sigma_{s,100\ Oe}$:

$$\boldsymbol{m}_{particle} = W_{particle}\times\sigma_{s,100Oe} = 6.77\times10^{-12}\ emu/particle \qquad \textbf{(equation S4)}$$

The values of $\boldsymbol{m}_{particle}$ for the ZFNPs and ZFMBs were estimated in a similar fashion. For the $\boldsymbol{m}_{particle}$ for Turbobeads, the field-dependent magnetization (***M-H*** curve) was obtained after the AC demagnetization procedure, due to their magnetic hysteresis.

Table S1. Calculation of $\boldsymbol{m}_{particle}$.

Particles	$\boldsymbol{m}_{particle}$ **at 100 Oe (emu/particle)**
Dynabeads	6.77×10^{-12}
Turbobeads	2.82×10^{-16}
ZFNP	5.35×10^{-17}
ZFMB	2.36×10^{-13}

3. Figures

3.1. TEM of as-synthesized ZFNPs and determination of Zn content in the ZFNPs.

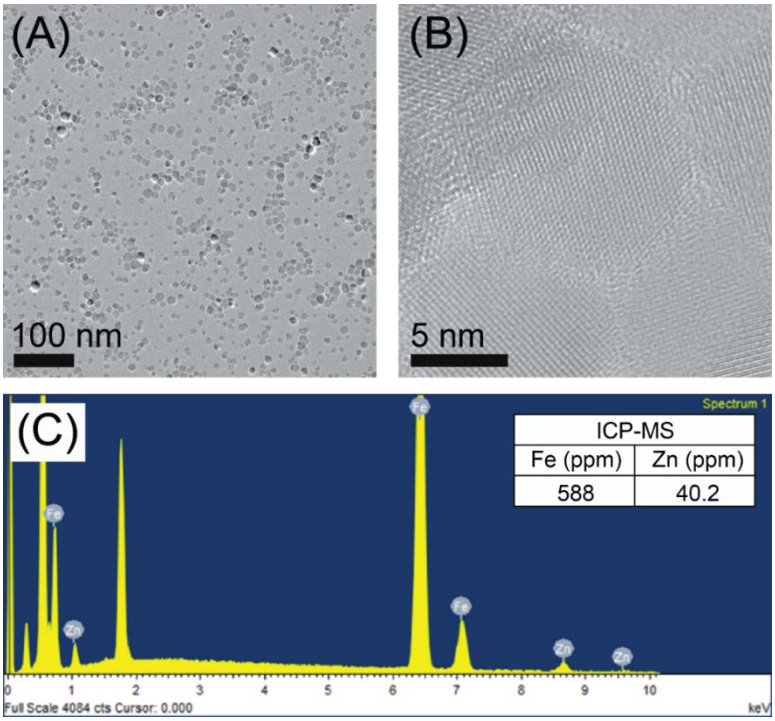

Figure S3. TEM and elemental analysis of the as-synthesized ZFNPs. High-resolution TEM image in (B) shows a lattice fringe pattern of the ZFNPs. EDS spectrum clearly shows the presence of Zn in the ZFNPs. The relative molar ratio of Zn to Fe in the as-synthesized ZFNPs, confirmed by inductively coupled plasma mass spectroscopy (ICP-MS), is 5.5:94.5 with 1% precision. This result agrees well with that from the analysis of the EDS data: the atomic ratio of Zn/Fe is 4.8/95.2.

3.2. SEM images of as-synthesized ZFMBs.

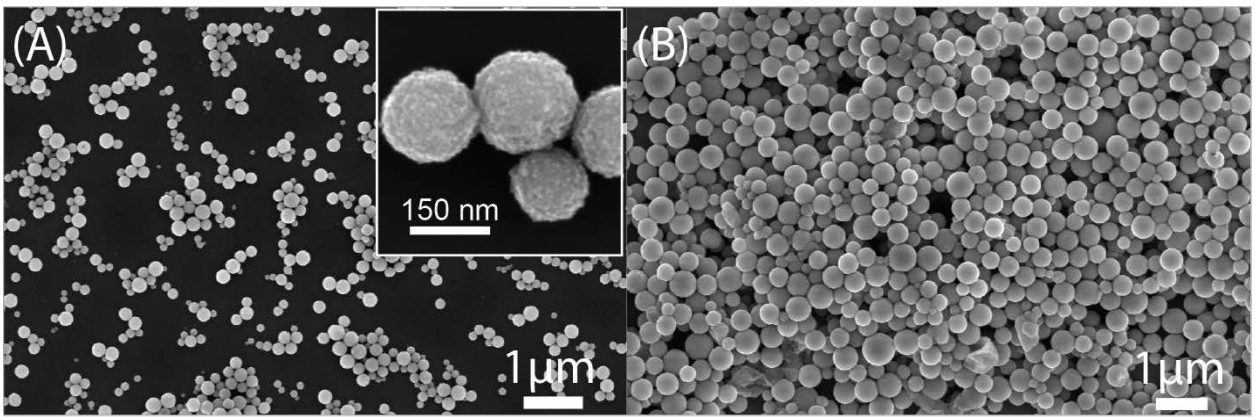

Figure S4. SEM images of as-synthesized ZFMBs with different sizes. The average diameters of (A) small and (B) large ZFMBs are 163 ± 46 and 378 ± 95 nm, respectively. Note that the average diameter was determined from SEM images by using ImageJ. The inset in (A) is a high-resolution SEM image, showing the distribution of ZFNPs at the surface of ZFMBs.

3.3. TEM and electron diffraction pattern of as-synthesized ZFMBs.

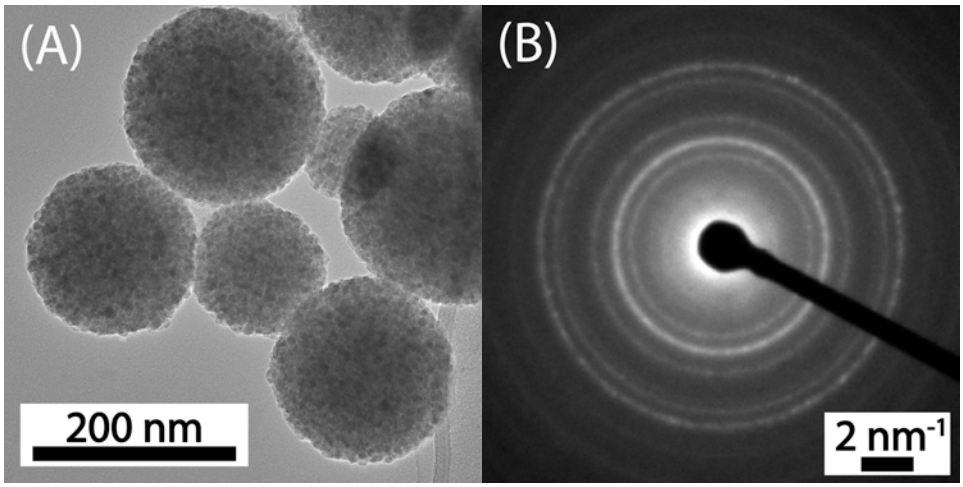

Figure S5. (A) TEM image and (B) electron diffraction pattern of the as-synthesized ZFMBs. Note that the TEM image (A) was acquired under an objective-lens defocus and that the superlattice fringe pattern with other types of superparticles[5-7] is not evident in our data.

3.4. Assignment of IR bands

Table S2. IR peak positions and band assignments of ZFNP and ZFMB particles.

mode assignment	description	band position (cm^{-1})
ν (Fe−O)	ferrite Fe−O lattice vibration	580−590
ν (C=O)	carbonyl stretching in PVP	1631−1664
δ (CH_2)	scissor bending in PVP, PAA, OA	1424−1462
ν (C−N)	carbon nitrogen stretching in PVP	1290
ν_a (COO^-)	asymmetric carboxylate stretching in PAA	1560−1562
ν_s (COO^-)	symmetric carboxylate stretching in PAA	1408−1413
ν (C=O)	carbonyl stretching in PAA	1690−1710
ν_a (CH_2)	asymmetric methylene stretching	2920
ν_s (CH_2)	symmetric methylene stretching	2850

3.5. Fluorescent microscopy of FITC-avidin tagged ZFMBs.

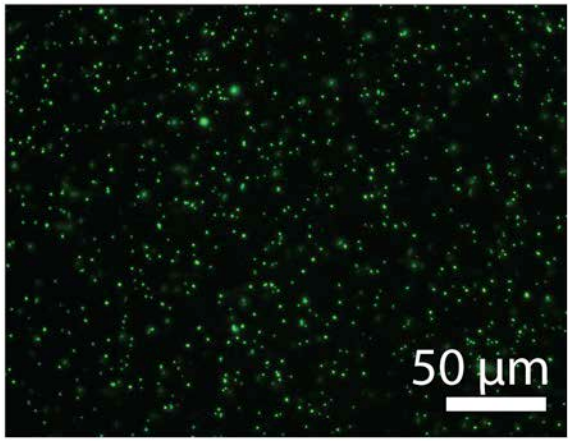

Figure S6. Fluorescent microscope images of the ZMBs conjugated with fluorescent molecule-tagged avidin (FITC-avidin). Scale bar is 20 µm. FITC-avidin molecules were conjugated to the ZFMBs@PVP@PAA using the same EDC/sulfo-NHS chemistry. A droplet of FITC-avidin conjugated ZFMBs in 5 mM MES (pH 6.5) was sandwiched between a microscope glass slide and a cover slip.

3.6. SEM images of Dynabeads and Turbobeads

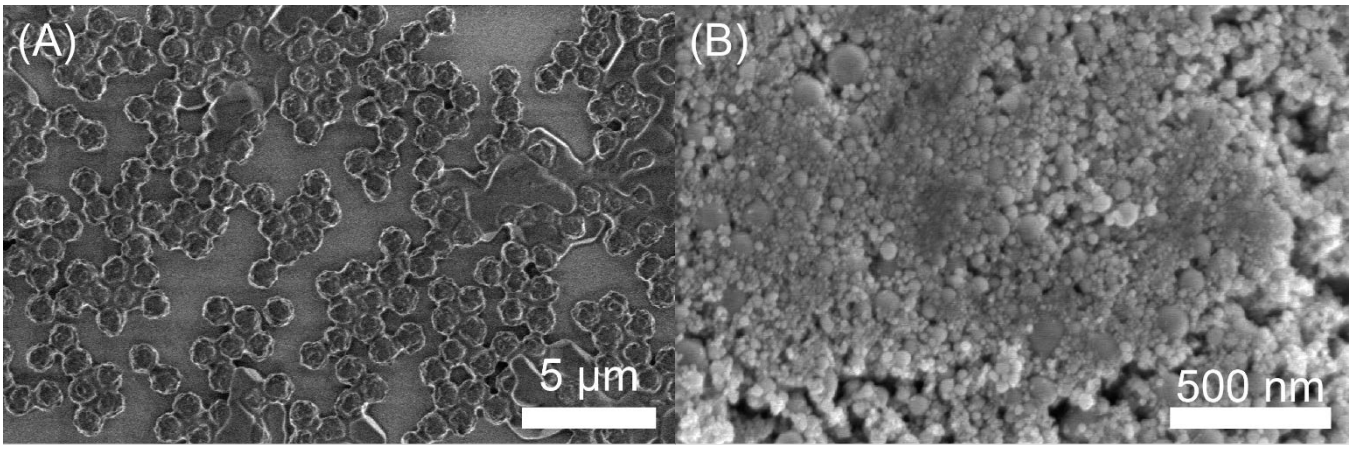

Figure S7. SEM images of commercially available streptavidinated magnetic beads: (A) Dynabeads and (B) Turbobeads. Dynabeads have a much higher uniformity in size than Turbobeads.

3.7. Optical microscope images and MR responses of OPN assays labeled with Dynabeads.

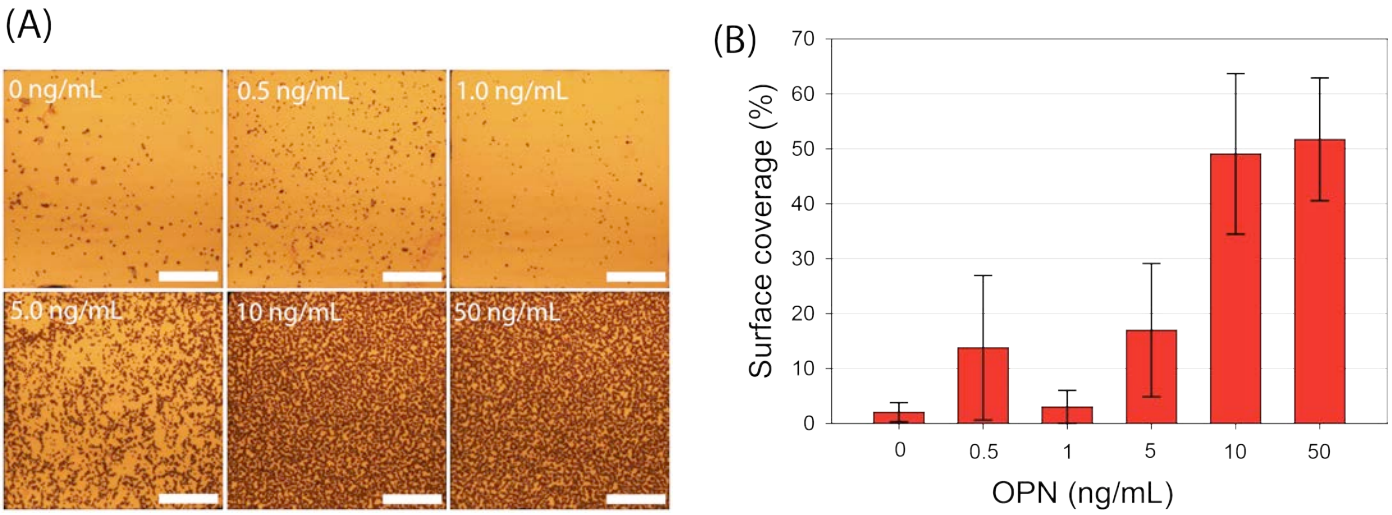

Figure S8. (A) Representative optical microscope images of gold addresses of OPN assays labeled with Dynabeads. Scale bar is 50 µm. (B) Average surface coverage of the Dynabeads as a function of OPN concentration. The average surface coverage was measured using ImageJ and calculated by averaging 12 gold addresses.

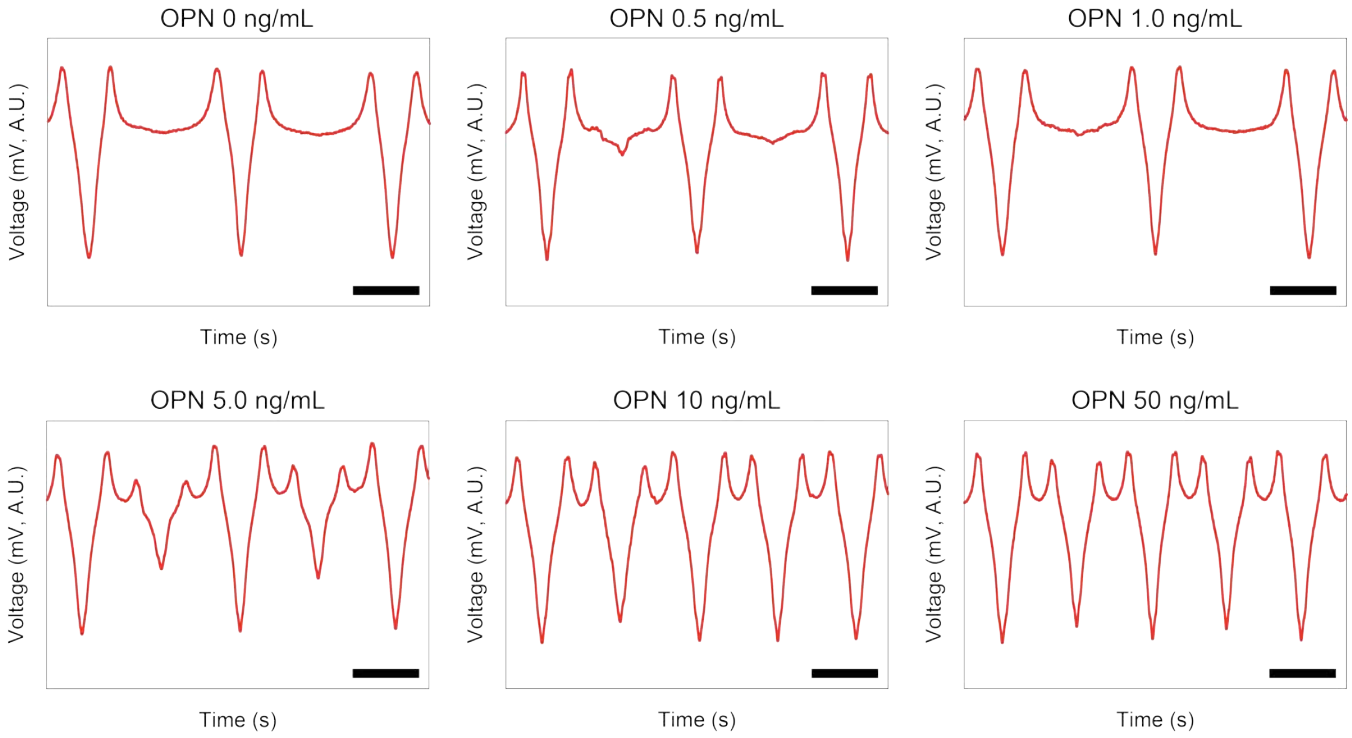

Figure S9. Representative MR signals of OPN assays labeled with Dynabeads. For simplicity, only two MR signals from gold addresses were plotted. Scale bar is 20 s.

3.8. Optical microscope images and MR responses of OPN assays labeled with streptavidinated ZFMBs.

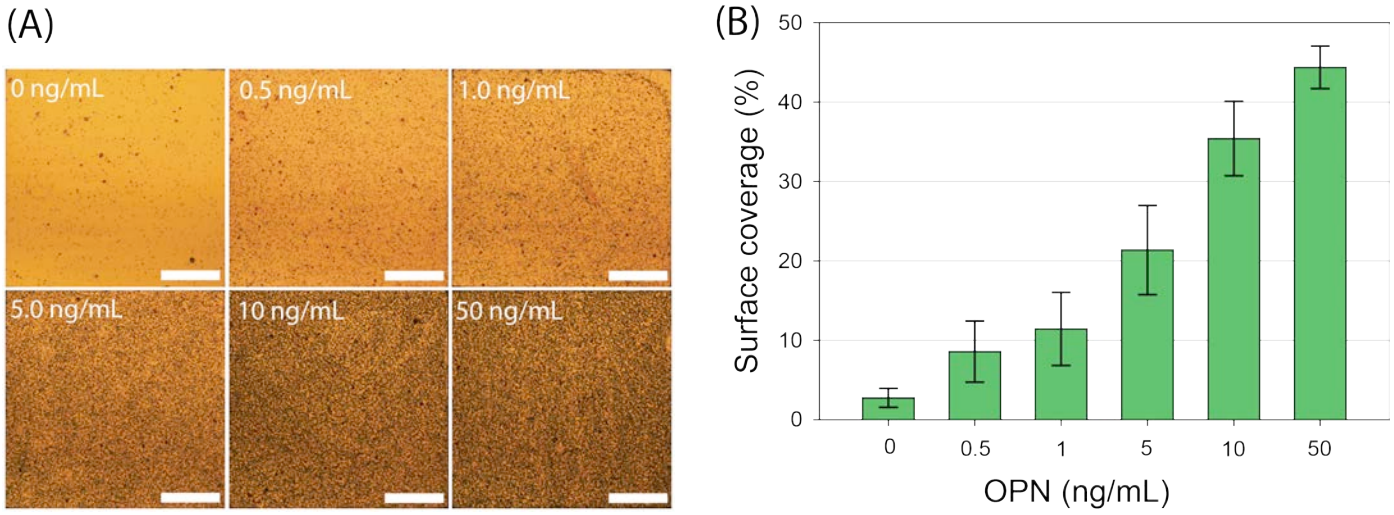

Figure S10. (A) Representative optical microscope images of gold addresses of OPN assays labeled with the streptavidinated ZFMBs. Scale bar is 50 µm. (B) Average surface coverage of the ZFMB labels as a function of OPN concentration. The average surface coverage was measured using ImageJ and calculated by averaging 12 gold addresses.

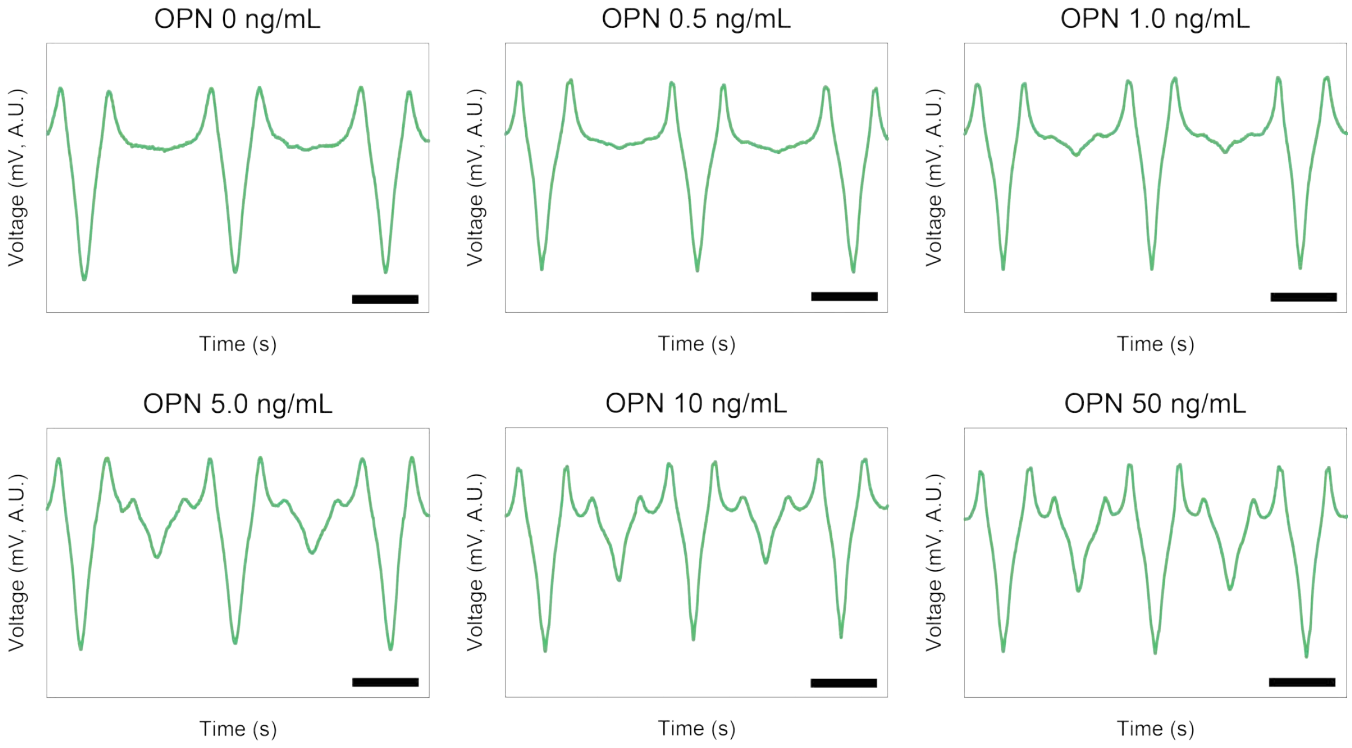

Figure S11. Representative MR signals of OPN assays labeled with the streptavidinated ZFMBs. For simplicity, only two MR signals from gold addresses were plotted. Scale bar is 20 s.

Author Information

Corresponding Author: * Michael.Granger@utah.edu.

Present Address: § M.C.G.: Sarcos Corporation, 360 Wakara Way, Salt Lake City, UT 84108

Reference

(1) Millen, R. L.; Nordling, J.; Bullen, H. A.; Porter, M. D.; Tondra, M.; Granger, M. C., Giant Magenetoresistive Sensors. 2. Detection of Biorecognition Events at Self-referencing and Magnetically Tagged Arrays. *Anal. Chem.* **2008,** *80*, 7940-7946.
(2) Nordling, J.; Millen, R. L.; Bullen, H. A.; Porter, M. D.; Tondra, M.; Granger, M. C., Giant Magnetoresistance Sensors. 1. Internally Calibrated Readout of Scanned Magnetic Arrays. *Anal. Chem.* **2008,** *80*, 7930-7939.
(3) Young, C. C.; Blackley, B. W.; Porter, M. D.; Granger, M. C., Frequency-Domain Approach To Determine Magnetic Address-Sensor Separation Distance Using the Harmonic Ratio Method. *Anal. Chem.* **2016,** *88*, 2015-2020.
(4) Rife, J.; Miller, M.; Sheehan, P.; Tamanaha, C.; Tondra, M.; Whitman, L., Design and performance of GMR sensors for the detection of magnetic microbeads in biosensors. *Sens. Actuators, A* **2003,** *107*, 209-218.
(5) Chen, O.; Riedemann, L.; Etoc, F.; Herrmann, H.; Coppey, M.; Barch, M.; Farrar, C. T.; Zhao, J.; Bruns, O. T.; Wei, H., Magneto-fluorescent Core-shell Supernanoparticles. *Nat. Commun.* **2014,** *5:5093*, 1-8.
(6) Chen, O.; Tan, R.; Zhu, H.; Cao, C., Multi-component Superstructures Self-assembled from Nanocrystal Building Blocks. *Nanoscale* **2016,** *8*, 9944-9961.
(7) Zhuang, J.; Wu, H.; Yang, Y.; Cao, Y. C., Controlling Colloidal Superparticle Growth through Solvophobic Interactions. *Angew. Chem. Int. Ed.* **2008,** *47*, 2208-2212.